JOURNAL OF GUIDANCE, CONTROL, AND DYNAMICS
Vol. 25, No. 6, November–December 2002

Adaptive Output Feedback for High-Bandwidth Flight Control

Nakwan Kim,* Anthony J. Calise,† Naira Hovakimyan,‡ and J. V. R. Prasad§
Georgia Institute of Technology, Atlanta, Georgia 30332-0150
and
Eric Corban¶
Guided Systems Technologies, Inc., McDonough, Georgia 30253

A novel adaptive output feedback approach for high-bandwidth flight-control system design is introduced. The approach permits adaptation to both parametric uncertainty and unmodeled dynamics. Of particular interest here is the interaction with poorly modeled high-frequency dynamics. An approximate output feedback linearizing controller is augmented with a neural network. Adaptation is achieved using input/output sequences of the uncertain system. Actuation limits and time delays are also addressed. The approach is illustrated by the design of a pitch-angle flight-control system for a linearized model of an R-50 experimental helicopter.

Nomenclature

$\bar{A}$	=	error dynamics system matrix
a	=	sigmoidal activation potential
$\boldsymbol{E}$	=	error dynamics state
$\hat{\boldsymbol{E}}$	=	error dynamics observer state
e	=	reference model tracking error
e_{com}	=	prefiltered command tracking error
e_{CRM}	=	reference model command tracking error
$f(\,)$	=	plant dynamics
$G_d(s)$	=	desired feedback linearized system transfer function
$h(\,)$	=	system output function
$h_i(\,)$	=	ith derivative of the system output function
$\hat{h}_i(\,)$	=	approximation of $h_i(\,)$
K	=	error dynamics observer gain
K_P, K_D	=	proportional gain and derivative gain of the dynamic compensator
k	=	σ-modification gain
N_1, N_2, N_3	=	number of neural network inputs, number of hidden-layer neurons, and number of outputs
n	=	dimension of the system
P, Q	=	positive definite matrices, reference model tracking Lyapunov equation
r	=	relative degree
u	=	control input variable
u_{cmd}	=	commanded control input
$\hat{u}$	=	estimated control input using a model for the actuator characteristics
v	=	total pseudocontrol
v_{ad}	=	neural network output
v_{DC}	=	dynamic compensator pseudocontrol component
v_h	=	hedge signal
v_{RM}	=	reference model pseudocontrol component
W, V, Z	=	neural network input and output weights
$\boldsymbol{x}$	=	state vector for plant dynamics
x_{RM}	=	reference model state
y	=	regulated output variable
y_{com}	=	prefiltered tracking command
y_{RM}	=	reference model output variable
$\bar{y}$	=	additional measurements that are available for feedback
Γ_W, Γ_V	=	diagonal matrices containing neural network learning rates
$\Delta(\,)$	=	model error function
$\hat{\delta}$, δ, δ_{cmd}	=	actuator position estimates, positions, and commands
ϵ	=	neural network reconstruction error
η	=	dynamic compensator state
$\lambda(\,)$	=	eigenvalue
$\boldsymbol{\mu}$	=	neural network input vector
$\boldsymbol{\xi}$	=	state vector associated with the output dynamics
$\boldsymbol{\sigma}(\,)$, $\sigma'(\,)$	=	neuron sigmoidal function and its gradient
$\boldsymbol{\chi}$	=	state vector associated with the zero dynamics
$\|\cdot\|_F$	=	Frobenius norm

Presented as Paper 2001-4181 at the AIAA Guidance, Navigation, and Control Conference, 6–9 August 2001; received 26 February 2002; revision received 22 July 2002; accepted for publication 24 July 2002.

*Graduate Research Assistant, School of Aerospace Engineering, 270 Ferst Drive. Student Member AIAA.
†Professor, School of Aerospace Engineering, 270 Ferst Drive. Fellow AIAA.
‡Research Scientist II, School of Aerospace Engineering, 270 Ferst Drive. Member AIAA.
§Professor, School of Aerospace Engineering, 270 Ferst Drive. Associate Fellow AIAA.
¶President, P.O. Box 1453. Member AIAA.

Introduction

MODERN fighter aircraft can be operated in highly nonlinear and uncertain flight conditions. In the future, uninhabited aerial vehicles (UAVs) will begin to displace inhabited aircraft in many traditional roles for both military and civilian missions. A challenge to designers of flight-control systems for future vehicles is to permit nearly carefree operation of high-performance vehicles, without limiting their full potential for maneuvering. Presently, there exists a gap between what is available and what can be achieved in UAV flight control, particularly in vehicles with hovering capabilities. We have been experimenting with numerous UAVs, and it has been our observation that a skilled human pilot can maneuver a small UAV in open loop at a level of proficiency that far exceeds the performance of an autonomous flight-control system. In flight-control research on an R-50 helicopter, it was observed that our pilot learns to anticipate and interact with high-frequency dynamics and delay when performing a demanding maneuvering task. The effective bandwidth of the control loop that is closed through the pilot in flying an otherwise open-loop vehicle exceeds, by roughly a factor of three, that which we are able to attain by providing rate command flight-control augmentation. This bandwidth limitation is largely due to control rotor dynamics (at approximately 8–10 rad/s), filtering, and digital processing time delays (between 0.02 and 0.04 s) that are present in the control path from the rate sensor to the main rotor swash plate. All physical systems also have control position and rate limits, which either deteriorate performance or destabilize it under high-bandwidth control.

Both classical and modern control design methods are fundamentally limited by the presence of unmodeled high-frequency effects. The same is particularly true in adaptive methods that attempt to learn and interact with these effects. It is the goal of our present research to develop an approach to flight-control design that is inspired by the performance levels that pilots are able to attain through long hours of training. This implies that we explicitly account for and adapt to the presence of unmodeled and potentially nonlinear dynamics in an output feedback setting, even if all of the states of the modeled portion of the system are available for feedback. Adaptation to unmodeled dynamics is achieved by recognizing the effect that these dynamics have in terms of both degree and relative degree of the system. Our main assumptions are that the system is minimum phase, stabilizable, and observable and that the relative degree of the regulated output variable is known. The dimension of the plant need not be known.

Feedback linearization[1,2] is a popular method for control of nonlinear systems. However, this approach relies on an accurate model for the system dynamics. Linearly parameterized neural networks (NN) (Ref. 3) have been used in combination with feedback linearization to compensate online for the error introduced by using an approximate inverting transformation. Stability analysis pertaining to control of affine nonlinear systems using nonlinearly parameterized networks first appeared using a discrete time formulation in Ref. 4 and using a continuous time formulation in Ref. 5. Applications in robotics are described in Ref. 6. Extensions to nonaffine systems, together with applications in flight control, can be found in Refs. 3 and 7–10.

Extensions of the methods just described to observer-based output feedback controls are treated in Refs. 11 and 12. However, these results to date are limited to systems with full relative degree (vector relative degree equals degree of the system) with the added constraint that the relative degree of each output is less than or equal to two.[13] In the single-input/single-output (SISO) case, this implies that observer-based adaptive output feedback control is limited to second-order systems with position measurement. Moreover, because state observers are employed, the dimension of the plant must be known. Therefore, methods that rely on a state observer are vulnerable to unmodeled dynamics. In Ref. 14 an error observer-based output feedback control design method is developed using only input/output sequences, which removes the limitations inherent in state observer-based design. Here, we extend it by incorporating a novel approach for treating control limits within an adaptive control setting called pseudocontrol hedging (PCH),[15] originally developed for the state feedback case.

We first state what is assumed to be known about the system dynamics, followed by a statement of the design objective. A summary of the main results on NN-based adaptive output feedback control via the error observer is given next, followed by a description of control architecture and the error observer design with hedging of the control limits. The paper concludes with an illustration of the main ideas by considering high-bandwidth pitch-attitude tracking control design for a linearized representation of the R-50 dynamics in hover, in which there is significant coupling with control rotor dynamics, actuator dynamics, control limits, and effects due to time delay. Results obtained using a full nonlinear model and recent flight-test results on our R-50 model helicopter are reported in Ref. 16. Steps used to demonstrate that all errors, error observer states, reference model command tracking errors, and network weights remain bounded are outlined in the Appendix.

Plant Description

Consider the following observable and stabilizable nonlinear SISO system:

$$\dot{\boldsymbol{x}} = \boldsymbol{f}(\boldsymbol{x}, u), \qquad y = h(\boldsymbol{x}) \tag{1}$$

where $\boldsymbol{x}$ is the state of the system on a domain $\mathcal{D}_x \subset R^n$, and $u, y \in R$ are the control and regulated output variables, respectively. The functions $\boldsymbol{f}$ and h may be unknown or approximately known. The regulated output is available for feedback, but there may be additional measurements $\bar{y}$ that are available also. This paper is applicable to SISO systems. However, the approach is easily modifed for multi-input/multi-output applications. See, for example, Refs. 10 and 17.

Assumption 1: The functions $\boldsymbol{f}: \mathcal{D}_x \times R \to R^n$ and $h: \mathcal{D}_x \to R$ are feedback linearizable,[2] and the output y has relative degree r for all $(\boldsymbol{x}, u) \in \mathcal{D}_x \times R$.

Based on this assumption, the mapping $\boldsymbol{\xi} = \boldsymbol{\Phi}(\boldsymbol{x})$ where

$$\boldsymbol{\Phi}(x) = \begin{bmatrix} L_f^0 h \\ L_f^1 h \\ \vdots \\ L_f^{(r-1)} h \end{bmatrix} \tag{2}$$

with $L_f^{(i)} h$, $i = 1, \ldots, r-1$ being the Lie derivatives, transforms system (1) into the so-called normal form[1]

$$\dot{\boldsymbol{\chi}} = f_0(\boldsymbol{\xi}, \boldsymbol{\chi}), \qquad \dot{\xi}_i = \xi_{i+1}, \qquad i = 1, \ldots, r-1$$
$$\dot{\xi}_r = h_r(\boldsymbol{\xi}, \boldsymbol{\chi}, u), \qquad y = \xi_1 \tag{3}$$

where $\boldsymbol{\xi} = [\xi_1 \ \cdots \ \xi_r]^T$, $h_r(\boldsymbol{\xi}, \boldsymbol{\chi}, u) = L_f^r h$, and $\boldsymbol{\chi}$ is the state vector associated with the zero dynamics

$$\dot{\boldsymbol{\chi}} = \boldsymbol{f}_0(0, \boldsymbol{\chi}) \tag{4}$$

Assumption 2: The zero dynamics in Eq. (4) are globally exponentially stable.

Controller Design and Tracking Error Dynamics

The control objective is to synthesize an output feedback control law such that $y(t)$ tracks a smooth bounded reference trajectory $y_{\mathrm{RM}}(t)$ with a bounded error using the available signals. Because the system is not exactly known and only y and $\bar{y}$ are available, feedback linearization is approximated by introducing the following control input signal:

$$u = \hat{h}_r^{-1}\left[y, \bar{y}, b_0 v - \sum_{i=0}^{r-1} a_i \hat{h}_i(y, \bar{y}) \right] \tag{5}$$

where v is commonly referred to as a pseudocontrol and b_0 and a_i are constants. The continuous function $\hat{h}_r(y, \bar{y}, u)$, which is required to be invertible with respect to its third argument, represents any available approximation of $h_r(\boldsymbol{x}, u) = L_f^r h$, and the continuous functions $\hat{h}_i(y, \bar{y})$ are approximations of $h_i(\boldsymbol{x}) = L_f^i h$. Additional requirements on $\hat{h}_r(y, \bar{y}, u)$ will be specified in assumption 3. Constants a_i and b_0 are determined later in the process of controller design.

With the available knowledge of the system dynamics, start by choosing approximate expressions for every derivative of the output up to rth derivative:

$$\begin{aligned} \dot{y} &= h_1(\boldsymbol{x}) = \hat{h}_1(y, \bar{y}) + \Delta_1 \\ \ddot{y} &= h_2(\boldsymbol{x}) = \hat{h}_2(y, \bar{y}) + \Delta_2 \\ &\vdots \\ y^{(r-1)} &= h_{r-1}(\boldsymbol{x}) = \hat{h}_{r-1}(y, \bar{y}) + \Delta_{r-1} \\ y^{(r)} &= h_r(\boldsymbol{x}, u) = \hat{h}_r(y, \bar{y}, u) + \Delta_r \end{aligned} \tag{6}$$

where Δ_i are model errors defined as $\Delta_i = h_i(\boldsymbol{x}) - \hat{h}_i(y, \bar{y})$ for $i = 1, 2, \ldots, r-1$ and $\Delta_r = h_r(\boldsymbol{x}, u) - \hat{h}_r(y, \bar{y}, u)$. If a linear model is used, then

$$y^{(i)} = c_i y + \bar{c}_i \bar{y} + \Delta_i, \qquad i = 1, \ldots, r-1$$
$$y^{(r)} = c_r y + \bar{c}_r \bar{y} + d_r u + \Delta_r \tag{7}$$

In the absence of any modeling information, we may select the approximation as $\hat{h}_1(y, \bar{y}) = \hat{h}_2(y, \bar{y}) = \cdots = \hat{h}_{r-1}(y, \bar{y}) = 0$ and $\hat{h}_r(y, \bar{y}, u) = d_r u$, subject to assumption 3.

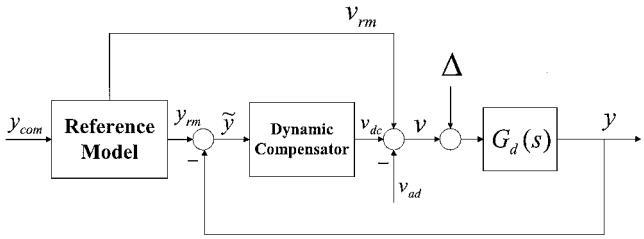

Fig. 1 Control system architecture.

To design the linear dynamic compensator, we need to specify the desired linearized system from v to y when $\Delta = 0$, $G_d(s)$ in Fig. 1, where

$$G_d(s) = b_0/D_d(s) \tag{8}$$

$$D_d(s) = s^r + a_{r-1}s^{r-1} + \cdots + a_1 s + a_0 \tag{9}$$

$G_d(s)$ should be considered together with the form of the dynamic compensator used to achieve a desired closed-loop level of performance.

Consider the model reference adaptive control architecture of Fig. 1. A dynamic compensator is designed to ensure that the resulting error dynamics, for $\Delta = 0$, are asymptotically stable and decay to zero faster than the desired response dynamics prescribed by the reference model. Combining Eqs. (8) and (9) for $\Delta \neq 0$ (see Fig. 1),

$$\begin{aligned} b_0(v+\Delta) &= y^{(r)} + a_{r-1}y^{(r-1)} + \cdots + a_1\dot{y} + a_0 y \\ &= \hat{h}_r(y, \bar{y}, u) + \Delta_r + a_{r-1}[\hat{h}_{r-1}(y, \bar{y}) + \Delta_{r-1}] \\ &\quad + \cdots + a_1[\hat{h}_1(y, \bar{y}) + \Delta_1] + a_0 y \\ &= \hat{h}_r(y, \bar{y}, u) + \sum_{i=0}^{r-1} a_i \hat{h}_i(y, \bar{y}) + \sum_{i=1}^{r} a_i \Delta_i \end{aligned} \tag{10}$$

where $\hat{h}_0(y) = y$, it can be seen that

$$v = \frac{1}{b_0}\left[\hat{h}_r(y, \bar{y}, u) + \sum_{i=0}^{r-1} a_i \hat{h}_i(y, \bar{y})\right] \tag{11}$$

$$\Delta = \frac{1}{b_0}\sum_{i=1}^{r} a_i \Delta_i \tag{12}$$

The control law (5) follows directly from Eq. (11). Applying the linear expressions in Eq. (7), we have

$$u = \frac{1}{d_r}\left[b_0 v - \sum_{i=0}^{r} a_i(c_i y + \bar{c}_r \bar{y})\right] \tag{13}$$

where $a_r = 1$, $c_0 = 1$, and $\bar{c}_0 = 0$.

The model inversion errors Δ_i can be regarded as continuous functions of $\boldsymbol{x}$ and v:

$$\Delta_i(\boldsymbol{x}) = h_i(x) - \hat{h}_i(y, \bar{y}) \qquad \text{for} \qquad i = 1, 2, \ldots, r-1$$

$$\begin{aligned} \Delta_r(\boldsymbol{x}, v) &= h_r(x, u) - \hat{h}_r(y, \bar{y}, u) \\ &= h_r\left\{\boldsymbol{x}, \hat{h}_r^{-1}\left[y, \bar{y}, b_0 v - \sum_{i=0}^{r-1} a_i \hat{h}_i(y, \bar{y})\right]\right\} \\ &\quad - \hat{h}_r\left\{y, \bar{y}, \hat{h}_r^{-1}\left[y, \bar{y}, b_0 v - \sum_{i=0}^{r-1} a_i \hat{h}_i(y, \bar{y})\right]\right\} \end{aligned} \tag{14}$$

Thus, the total model inversion error is a continuous function of $\boldsymbol{x}$ and v:

$$\Delta(\boldsymbol{x}, v) = \frac{1}{b_0}\left[\Delta_r(\boldsymbol{x}, v) + \sum_{i=1}^{r-1} a_i \Delta_i(\boldsymbol{x})\right] \tag{15}$$

The pseudocontrol in Eq. (5) is chosen to have the form

$$v = v_{\mathrm{RM}} + v_{\mathrm{DC}} - v_{\mathrm{ad}} \tag{16}$$

where v_{RM} is a reference model output, v_{DC} is the output of a linear dynamic compensator, and v_{ad} is the adaptive control signal. With the choice of pseudocontrol in Eq. (16), the dynamics in Eq. (10) reduce to

$$\sum_{i=0}^{r} a_i y^{(i)} = b_0(v_{\mathrm{RM}} + v_{\mathrm{DC}} - v_{\mathrm{ad}} + \Delta), \qquad a_r = 1 \tag{17}$$

From Eqs. (15) and (17), note that Δ depends on v_{ad} through v and that the role of v_{ad} is to cancel Δ. The following assumption is introduced to guarantee the existence and uniqueness of a solution for v_{ad} (Ref. 18):

Assumption 3: The mapping $v_{\mathrm{ad}} \mapsto \Delta$ is a contraction over the entire input domain of interest.

A contraction is defined by the following condition:

$$\left|\frac{\partial \Delta}{\partial v_{\mathrm{ad}}}\right| < 1 \tag{18}$$

When Eq. (15) is used, the condition in condition (18) implies

$$\begin{aligned} \left|\frac{\partial \Delta}{\partial v_{\mathrm{ad}}}\right| &= \left|\frac{1}{b_0}\frac{\partial \Delta_r}{\partial v_{\mathrm{ad}}}\right| = \left|\frac{1}{b_0}\frac{\partial(h_r - \hat{h}_r)}{\partial u}\frac{\partial u}{\partial v}\frac{\partial v}{\partial v_{\mathrm{ad}}}\right| \\ &= \left|\frac{1}{b_0}\frac{\partial(h_r - \hat{h}_r)}{\partial u}\frac{b_0 \partial u}{\partial \hat{h}_r}\right| < 1 \end{aligned} \tag{19}$$

which can be rewritten as follows:

$$\left|\frac{\partial h_r/\partial u}{\partial \hat{h}_r/\partial u} - 1\right| < 1 \tag{20}$$

Condition (20) is satisfied if the following two conditions hold:

$$\mathrm{sgn}\left(\frac{\partial \hat{h}_r}{\partial u}\right) = \mathrm{sgn}\left(\frac{\partial h_r}{\partial u}\right) \tag{21}$$

$$0 < \frac{1}{2}\left|\frac{\partial h_r}{\partial u}\right| < \left|\frac{\partial \hat{h}_r}{\partial u}\right| < \infty \tag{22}$$

Condition (21) requires that the sign of the control effectiveness is known, and condition (22) places a lower bound on its estimate

$$\mathrm{sgn}(d_r) = \mathrm{sgn}\left(\frac{\partial h_r}{\partial u}\right), \qquad 0 < \frac{1}{2}\left|\frac{\partial h_r}{\partial u}\right| < |d_r| < \infty \tag{23}$$

Thus, it is better to overestimate the control effectiveness to satisfy assumption 3.

Define the reference model pseudocontrol v_{RM}:

$$\begin{aligned} v_{\mathrm{RM}} &= [1/G_d(s)]y_{\mathrm{RM}} = [D_d(s)/b_0]y_{\mathrm{RM}} \\ &= (1/b_0)\left(y_{\mathrm{RM}}^{(r)} + a_{r-1}y_{\mathrm{RM}}^{(r-1)} + \cdots + a_1\dot{y}_{\mathrm{RM}} + a_0 y_{\mathrm{RM}}\right) \end{aligned} \tag{24}$$

Then the dynamics in Eq. (17) can be rewritten:

$$\sum_{i=0}^{r} a_i e^{(i)} + b_0(v_{\mathrm{DC}} - v_{\mathrm{ad}} + \Delta) = 0 \tag{25}$$

where $e = y_{\mathrm{RM}} - y$. When v_{ad} cancels Δ, or for $v_{\mathrm{ad}} = \Delta = 0$, the error dynamics in Eq. (25) reduces to

$$D_d(s)e + b_0 v_{\mathrm{DC}} = 0 \tag{26}$$

For the case $r > 1$, the following linear dynamic compensator is introduced to stabilize the dynamics in Eq. (26):

$$\dot{\boldsymbol{\eta}} = A_c\boldsymbol{\eta} + \boldsymbol{b}_c e, \qquad \boldsymbol{\eta} \in R^{n_c}, \qquad v_{\mathrm{DC}} = \boldsymbol{c}_c\boldsymbol{\eta} + d_c e \tag{27}$$

Returning to Eq. (25), the vector $\boldsymbol{e} = [e \;\; \dot{e} \;\; \cdots \;\; e^{(r-1)}]^T$, together with the compensator state $\boldsymbol{\eta}$, will obey the following dynamics, hereafter referred to as the tracking error dynamics:

$$\begin{bmatrix} \dot{\boldsymbol{e}} \\ \dot{\boldsymbol{\eta}} \end{bmatrix} = \begin{bmatrix} A - \boldsymbol{b}(b_0 d_c \boldsymbol{c} + \boldsymbol{a}) & -b_0 \boldsymbol{b} \boldsymbol{c}_c \\ \boldsymbol{b}_c \boldsymbol{c} & A_c \end{bmatrix} \begin{bmatrix} \boldsymbol{e} \\ \boldsymbol{\eta} \end{bmatrix} + \begin{bmatrix} \boldsymbol{b} \\ 0 \end{bmatrix} b_0 (v_{\text{ad}} - \Delta)$$

$$\boldsymbol{z} \triangleq [e \quad \boldsymbol{\eta}^T]^T \tag{28}$$

where

$$A = \begin{bmatrix} 0 & 1 & 0 & \cdots & 0 \\ 0 & 0 & 1 & & 0 \\ \vdots & \vdots & & \ddots & \\ 0 & 0 & & & 1 \\ 0 & 0 & 0 & \cdots & 0 \end{bmatrix}, \qquad \boldsymbol{b} = \begin{bmatrix} 0 \\ 0 \\ \vdots \\ 0 \\ 1 \end{bmatrix}$$

$$\boldsymbol{c} = [1 \quad 0 \quad 0 \quad \cdots \quad 0], \qquad \boldsymbol{a} = [a_0 \quad a_1 \quad \cdots \quad a_{r-1}] \tag{29}$$

with appropriate dimensions, and $\boldsymbol{z}$ is a vector of available signals. For ease of notation, define the following matrices:

$$\bar{A} = \begin{bmatrix} A - \boldsymbol{b}(b_0 d_c \boldsymbol{c} + \boldsymbol{a}) & -b_0 \boldsymbol{b} \boldsymbol{c}_c \\ \boldsymbol{b}_c \boldsymbol{c} & A_c \end{bmatrix}$$

$$\bar{\boldsymbol{b}} = \begin{bmatrix} \boldsymbol{b} \\ 0 \end{bmatrix}, \qquad \bar{C} = \left[\begin{array}{c|c} \boldsymbol{c} & 0 \\ \hline 0 & I \end{array}\right] \tag{30}$$

and a new vector

$$\boldsymbol{E} \triangleq \begin{bmatrix} \boldsymbol{e} \\ \boldsymbol{\eta} \end{bmatrix} \tag{31}$$

With these definitions, the tracking error dynamics in Eq. (28) can be rewritten as

$$\dot{\boldsymbol{E}} = \bar{A}\boldsymbol{E} + \bar{\boldsymbol{b}} b_0 (v_{\text{ad}} - \Delta), \qquad \boldsymbol{z} = \bar{C}\boldsymbol{E} \tag{32}$$

where it has already been noted that $A_c, \boldsymbol{b}_c, \boldsymbol{c}_c, d_c$ should be designed such that $\bar{A}$ is Hurwitz.

Design and Analysis of an Observer for the Error Dynamics

In the case of full state feedback,[9,10,19] Lyapunov-like stability analysis of the error dynamics in Eq. (32) results in update laws for the adaptive control parameters in terms of the error vector $\boldsymbol{E}$. In Refs. 11–13, an adaptive state observer is developed for the nonlinear plant to provide state estimates needed in the adaptation laws. However, the stability analysis was limited to second-order systems with position measurements. To relax these assumptions, we make use of a simple linear observer for the tracking error dynamics in Eq. (32) (Refs. 14 and 20). This observer provides estimates of the unavailable error signals for the update laws of the adaptive parameters that will be presented in Eq. (66).

Consider the following full-order linear observer for the tracking error dynamic system in Eq. (32):

$$\dot{\hat{\boldsymbol{E}}} = \bar{A}\hat{\boldsymbol{E}} + K(\boldsymbol{z} - \hat{\boldsymbol{z}}), \qquad \hat{\boldsymbol{z}} = \bar{C}\hat{\boldsymbol{E}} \tag{33}$$

where K should be chosen in a way to make $\bar{A} - K\bar{C}$ asymptotically stable. The following remarks will be useful in the sequel:

Remark 1: Notice that Eq. (33) provides estimates only for the states that are feedback linearized and not for the states that are associated with the zero dynamics.

Remark 2: One can also design an r-2 dimensional minimal-order observer, or a minimal-order optimal estimator that treats the $\boldsymbol{\eta}$ component of $\boldsymbol{z}$ as a noiseless measurement.

Remark 3: Additional measurements contained in $\bar{y}$ may also be used both in the compensator design and in the observer design. This idea is employed in the application.

This observer design ignores the nonlinearities that enter the tracking error dynamics (32) as a forcing function. This is suggested by the original nonlinear system being approximately feedback linearized, or by v_{ad} nearly canceling Δ, and is justified using Lyapunov's direct method in the Appendix.

Let

$$\tilde{A} \triangleq \bar{A} - K\bar{C}, \qquad \tilde{\boldsymbol{E}} \triangleq \hat{\boldsymbol{E}} - \boldsymbol{E} \tag{34}$$

Then the observer error dynamics can be written

$$\dot{\tilde{\boldsymbol{E}}} = \tilde{A}\tilde{\boldsymbol{E}} - \bar{\boldsymbol{b}} b_0 [v_{\text{ad}} - \Delta] \tag{35}$$

NN Approximation of the Inversion Error

The term "artificial NN" has come to mean any architecture that has massively parallel interconnections of simple "neural" processors. Given $\boldsymbol{x} \in R^{N_1}$, a three-layer NN has an output given by

$$y_i = \sum_{j=1}^{N_2} \left[w_{ij} \sigma \left(\sum_{k=1}^{N_1} v_{jk} x_k + \theta_{vj} \right) + \theta_{wi} \right], \qquad i = 1, \ldots, N_3 \tag{36}$$

where $\sigma(\,)$ is the activation function, v_{jk} are the first-to-second layer interconnection weights, w_{ij} are the second-to-third layer interconnection weights, and θ_{vj} and θ_{wi} are bias terms. Such an architecture is known to be a universal approximator of piecewise continuous nonlinearities with "squashing" activation functions.[21]

The following theorem extends these results to map the unknown dynamics of an observable plant from available input/output history.

Theorem 1: Given $\epsilon^* > 0$ and the compact set $\mathcal{D} \subset \mathcal{D}_x \times R$, there exists a set of bounded weights V^*, W^* with N_2 sufficiently large such that the continuous function $\Delta(\boldsymbol{x}, v)$ in Eq. (15) can be approximated by a three-layer NN

$$\Delta(\boldsymbol{x}, v) = W^{*T} \boldsymbol{\sigma}(V^{*T} \boldsymbol{\mu}) + \epsilon(\boldsymbol{\mu}), \qquad \|\epsilon\| < \epsilon^* \tag{37}$$

using the input vector

$$\boldsymbol{\mu}(t) = \begin{bmatrix} 1 & \boldsymbol{v}_d^T(t) & \boldsymbol{y}_d^T(t) \end{bmatrix}^T \tag{38}$$

where

$$\boldsymbol{v}_d^T(t) = \{v(t), v(t-d), \ldots, v[t - (n_1 - r - 1)d]\}^T$$

$$\boldsymbol{y}_d^T(t) = \{y(t), y(t-d), \ldots, y[t - (n_1 - 1)d]\}^T$$

with $n_1 \geq n$ and $d > 0$, $\boldsymbol{\sigma}$ is any squashing function.

Proof: See Ref. 18.

The input/output history of the original nonlinear plant is needed to map Δ in systems with zero dynamics because for such systems the unobservable subspace is not estimated by Eq. (33), but can be accounted for by the input/output history, as noted in remark 1. If the system has full relative degree, the observer in Eq. (33) provides all of the estimates needed for the reconstruction of Δ, and no past input/output history is required.[20]

Remark 4: The inversion error Δ is defined on $\mathcal{D} \subset \mathcal{D}_x \times R \subset R^{n+1}$, whereas the input vector to the NN in Eq. (38) belongs to $\mathcal{D}_\mu \subset R^{2n_1 - r + 1}$.

The adaptive term in Eq. (16) is designed as

$$v_{\text{ad}} = W^T \boldsymbol{\sigma}(V^T \boldsymbol{\mu}) \tag{39}$$

where W and V are the NN weights to be updated on line. With squashing functions that are continuous and monotonic, Eq. (39) will always have at least one fixed-point solution for v_{ad}.

Define

$$\tilde{W} \triangleq W - W^*, \qquad \tilde{V} \triangleq V - V^*, \qquad \tilde{Z} \triangleq \begin{bmatrix} \tilde{W} & 0 \\ 0 & \tilde{V} \end{bmatrix} \tag{40}$$

and note that

$$\|W\|_F < \|\tilde{W}\|_F + \bar{W}, \qquad \|V\|_F < \|\tilde{V}\|_F + \bar{V} \tag{41}$$

where $\bar{W}$ and $\bar{V}$ are the upper bounds for the weights in Eq. (37):

$$\|W^*\|_F < \bar{W}, \qquad \|V^*\|_F < \bar{V} \tag{42}$$

With condition (41), the representation

$$v_{\text{ad}} - \Delta = W^T\boldsymbol{\sigma}(V^T\boldsymbol{\mu}) - W^{*T}\boldsymbol{\sigma}(V^{*T}\boldsymbol{\mu}) - \epsilon \tag{43}$$

allows for the following upper bound for some computable γ_1 and γ_2:

$$\|v_{\text{ad}} - \Delta\| \le \gamma_1\|\tilde{Z}\|_F + \gamma_2, \qquad \gamma_1 > 0, \qquad \gamma_2 > 0 \tag{44}$$

For the stability proof, we will need the following representation:

$$W^T\boldsymbol{\sigma}(V^T\boldsymbol{\mu}) - W^{*T}\boldsymbol{\sigma}(V^{*T}\boldsymbol{\mu})$$

$$= \tilde{W}^T(\boldsymbol{\sigma} - \hat{\sigma}'V^T\boldsymbol{\mu}) + W^T\sigma'\tilde{V}^T\boldsymbol{\mu} + w \tag{45}$$

where $\boldsymbol{\sigma} = \boldsymbol{\sigma}(V\boldsymbol{\mu})$, $\sigma'(z) = \text{diag}\,(\text{d}\sigma_i/\text{d}z_i)$ and $w = \tilde{W}^T\sigma'V^{*T}\boldsymbol{\mu} - W^{*T}\mathcal{O}^2(\tilde{V}^T\boldsymbol{\mu})$. This representation is achieved via Taylor series expansion of $\boldsymbol{\sigma}(V^{*T}\boldsymbol{\mu})$ around the estimates $V^T\boldsymbol{\mu}$. (See Ref. 19 for more details.) The following assumption is used in the stability analysis:

Assumption 4: The input vector to the NN is uniformly bounded on $\mathcal{D}_\mu$

$$\|\boldsymbol{\mu}\| \le \mu^*, \qquad \mu^* > 0 \tag{46}$$

A bound for $(w - \epsilon)$ over the compact set $\mathcal{D}_\mu$ can be expressed as follows[19]:

$$\|w - \epsilon\| \le \gamma_1\|\tilde{Z}\|_F + \gamma_2, \qquad \gamma_1 > 0, \qquad \gamma_2 > 0 \tag{47}$$

where γ_1 and γ_2 are constants that depend on μ^* and ϵ^*. Thus, the forcing term in Eq. (32) can be written

$$v_{\text{ad}} - \Delta = \tilde{W}^T(\boldsymbol{\sigma} - \sigma'V^T\boldsymbol{\mu}) + W^T\sigma'\tilde{V}^T\boldsymbol{\mu} + w - \epsilon \tag{48}$$

subject to conditions (46) and (47).

PCH

Adaptive controllers are sensitive to input nonlinearities such as actuator position limits, actuator rate limits, actuator dynamics, and time delay. The concept of hedging the reference model to prevent an adaptive law from seeing (attempting to adapt to) these unfavorable system characteristics was introduced in Ref. 15. This approach permits adaptation even during periods of control saturation (when not in control). A pseudocontrol hedge v_h is obtained by first estimating the actuator position $\hat{u}$ using a model for the actuator characteristics. This estimate is then used to compute the difference between commanded pseudocontrol v and the estimated achievable pseudocontrol. The process is illustrated in Fig. 2 for an actuator model that has position limits, rate limits, actuator dynamics, and time delay. With Eq. (11), v_h, the PCH signal, can be expressed as

$$v_h = v - \frac{1}{b_0}\left\{\hat{h}_r(y, \bar{y}, \hat{u}) + \sum_{i=0}^{r-1} a_i\hat{h}_i(y, \bar{y})\right\}$$

$$= \frac{1}{b_0}\{\hat{h}_r(y, \bar{y}, u_{\text{cmd}}) - \hat{h}_r(y, \bar{y}, \hat{u})\} \tag{49}$$

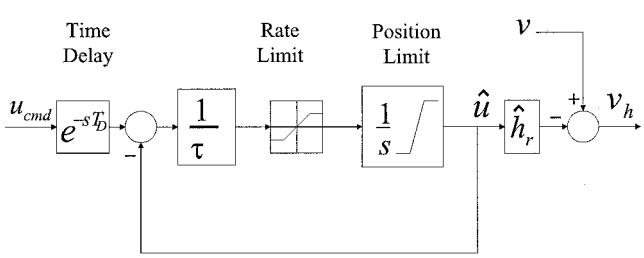

Fig. 2 Computation of the PCH signal.

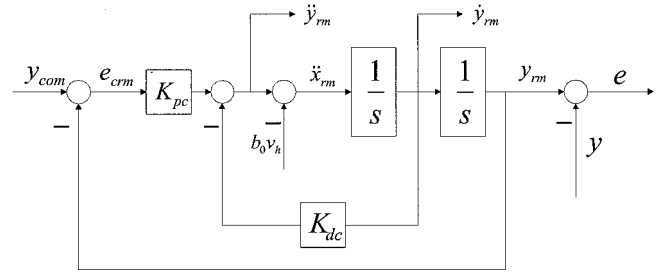

Fig. 3 Second-order reference model with PCH signal.

where u_{cmd} is commanded control input from Eq. (5) and $\hat{u}$ is the estimated control input depicted in Fig. 2. The PCH signal is then subtracted from the reference model dynamics as described by the following equation:

$$x_{\text{RM}}^{(r)} = f_{\text{RM}}\left(x_{\text{RM}}, \dot{x}_{\text{RM}}, \ldots, x_{\text{RM}}^{(r-1)}, y_{\text{com}}\right) - b_0v_h \tag{50}$$

where y_{com} is the unfiltered command signal. The manner in which it is incorporated in a linear reference model is shown in Fig. 3 for the case $r = 2$. The second-order reference model augmented with the PCH signal can be expressed in the following state-space form:

$$\begin{bmatrix}\dot{x}_{\text{RM}}\\ \ddot{x}_{\text{RM}}\end{bmatrix} = \underbrace{\begin{bmatrix}0 & 1\\ -K_{\text{PC}} & -K_{\text{DC}}\end{bmatrix}}_{A_{\text{RM}}}\begin{bmatrix}x_{\text{RM}}\\ \dot{x}_{\text{RM}}\end{bmatrix} + \underbrace{\begin{bmatrix}0 & 0\\ K_{\text{PC}} & -b_0\end{bmatrix}}_{B_{\text{RM}}}\begin{bmatrix}y_{\text{com}}\\ v_h\end{bmatrix}$$

$$\begin{bmatrix}y_{\text{RM}}\\ \dot{y}_{\text{RM}}\\ \ddot{y}_{\text{RM}}\end{bmatrix} = \begin{bmatrix}1 & 0\\ 0 & 1\\ -K_{\text{PC}} & -K_{\text{DC}}\end{bmatrix}\begin{bmatrix}x_{\text{RM}}\\ \dot{x}_{\text{RM}}\end{bmatrix} + \begin{bmatrix}0 & 0\\ 0 & 0\\ K_{\text{PC}} & 0\end{bmatrix}\begin{bmatrix}y_{\text{com}}\\ v_h\end{bmatrix} \tag{51}$$

where K_{PC} and K_{DC} are the reference model gains chosen such that A_{RM} is Hurwitz.

Ultimate Boundedness

This section addresses ultimate boundedness of the errors in reference model states, NN weights, plant states, and error observer states. To establish this result, we follow the rationale developed in Refs. 14 and 15. In Ref. 14, ultimate boundedness of error signals has been shown in an output feedback setting using Lyapunov's direct method for the case of unbounded actuation. In Ref. 15, ultimate boundedness of error signals in the presence of actuation limits have been shown for the state feedback case. Here we develop a synergy of the proofs laid out in Refs. 14 and 15 to account for system input characteristics and PCH in an output feedback setting. We show that all error signals are uniformly ultimately bounded, provided that upper/lower bounds for the adaptation gains are respected.

We first consider an isolated nonadaptive system and then combine it with the adaptive system later as suggested in Ref. 15. The error states that will be used in the proof of boundedness are shown in Fig. 3:

$$e = y_{\text{RM}} - y, \qquad e_{\text{com}} = y_{\text{com}} - y, \qquad e_{\text{CRM}} = y_{\text{com}} - y_{\text{RM}} \tag{52}$$

where y_{com} is the prefiltered command and y_{RM} is the filtered signal through the reference model. The isolated nonadaptive system represents the plant when reference model tracking error e is zero, $v_{\text{ad}} = \Delta$, and $e_{\text{com}} = e_{\text{CRM}}$. For $r = 2$, the reference model command error dynamics is given by

$$\dot{\boldsymbol{E}}_{\text{CRM}} = A_{\text{RM}}\boldsymbol{E}_{\text{CRM}} + \begin{bmatrix}0\\ \ddot{y}_{\text{com}} + K_{\text{DC}}\dot{y}_{\text{com}}\end{bmatrix} \tag{53}$$

where $\boldsymbol{E}_{\text{CRM}} = [y_{\text{com}} - y_{\text{RM}},\ \dot{y}_{\text{com}} - \dot{y}_{\text{RM}}]^T$ with A_{RM} defined in Eq. (51).

Assumption 5: There exists a Lyapunov function for an isolated nonadaptive part of the overall system.

When considering the isolated system design for the nonadaptive subsystem, reference model tracking error is zero

($e_{com} = e_{CRM}$), and we can take $L_{CRM}(\boldsymbol{E}_{CRM}) = \boldsymbol{E}_{CRM}^T P_{CRM} \boldsymbol{E}_{CRM}$ as a candidate Lyapunov function for the subsystem, where P_{CRM} is the positive-definite solution to the Lyapunov equation $A_{RM}^T P_{CRM} + P_{CRM} A_{RM} + Q_{CRM} = 0$ with $\lambda_{min}(Q_{CRM}) \geq \gamma > 0$. The derivative of L_{CRM} along Eq. (53) will be

$$\dot{L}_{CRM}(\boldsymbol{E}_{CRM}) \leq -\boldsymbol{E}_{CRM}^T Q_{CRM} \boldsymbol{E}_{CRM} + 2\|\boldsymbol{E}_{CRM}\| \|P_{CRM} \bar{y}_{com}\|$$

$$\leq -\lambda_{min}(Q_{CRM}) \|\boldsymbol{E}_{CRM}\|^2 + 2\gamma \|\boldsymbol{E}_{CRM}\| \leq 0 \tag{54}$$

where $\bar{y}_{com} = [0, \ddot{y}_{com} + K_{DC} \dot{y}_{com}]^T$, $\gamma = \|P_{CRM} \bar{y}_{com}\|$, and $\lambda_{min}(Q_{CRM})$ is the minimum eigenvalue of Q_{CRM}.

Consider the following vector:

$$\zeta = \left[\boldsymbol{E}_{CRM}^T, \boldsymbol{E}^T, \tilde{\boldsymbol{E}}^T, \text{vec}\tilde{Z}^T\right]^T \tag{55}$$

Notice that it can be viewed as a function of the state variables $\boldsymbol{x}$, $\boldsymbol{\eta}$, $\hat{\boldsymbol{E}}$, and Z; the reference model vectors $\boldsymbol{y}_{RM}$ and y_{com}; and the constant matrix Z^*:

$$\zeta = \boldsymbol{F}\left(\boldsymbol{x}, \boldsymbol{y}_{com}, \boldsymbol{y}_{RM}, \boldsymbol{\eta}, \hat{\boldsymbol{E}}, Z, Z^*\right) \tag{56}$$

where

$$Z = \begin{bmatrix} W & 0 \\ 0 & V \end{bmatrix}, \qquad Z^* = \begin{bmatrix} W^* & 0 \\ 0 & V^* \end{bmatrix}$$

and $\mathcal{D}_{y_{com}}$ and $\mathcal{D}_{Z^*}$ are assumed to be bounded. Recall that Eq. (37) introduces the compact set $\mathcal{D}$ over which the NN approximation is valid. From Eq. (37), it follows that

$$[\boldsymbol{x}^T \quad v]^T \in \mathcal{D} \Rightarrow \boldsymbol{x} \in \mathcal{D}_x, \qquad v \in \mathcal{D}_v \tag{57}$$

where $\mathcal{D}_x$ and $\mathcal{D}_v$ are bounded. According to Eq. (16)

$$v = \boldsymbol{F}_v(\boldsymbol{\eta}, \boldsymbol{\mu}, Z, \boldsymbol{y}_{RM}) \tag{58}$$

where $\boldsymbol{F}_v : \mathcal{D}_\eta \times \mathcal{D}_\mu \times \mathcal{D}_Z \times \mathcal{D}_{yRM} \to \mathcal{D}_v$. This implies that $\mathcal{D}_\eta$, $\mathcal{D}_\mu$, $\mathcal{D}_Z$, and $\mathcal{D}_{yRM}$ are bounded. $\mathcal{D}_{\hat{E}}$ is also bounded because the error observer in Eq. (33) is asymptotically stable and driven by $\boldsymbol{E}$, which is a function defined on bounded sets $\mathcal{D}_x \times \mathcal{D}_{yRM} \times D_\eta$. The relation in Eq. (56) represents a mapping from the bounded sets to $\mathcal{D}_\zeta$ in the error space. We can conclude that the set $\mathcal{D}_\zeta$ in the error space is bounded and introduce the largest convex compact set that is contained in $\mathcal{D}_\zeta$, such that

$$B_r \triangleq \{\zeta : \|\zeta\| \leq r\}, \qquad r > 0 \tag{59}$$

We want to ensure that a Lyapunov function level set Ω_β is an ultimate bound for the error ζ in $\mathcal{D}_\zeta$ by showing that the level set Ω_β inside B_r contains a compact set Γ, outside of which a time derivative of the Lyapunov function candidate is negative, as is shown later. A Lyapunov function level set Ω_α is introduced to ensure that Ω_β is contained in B_r, and a ball B_c is introduced to provide that Ω_β contains Γ. Before we state the theorem, we state an assumption that will be used in the proof of the theorem.

Assumption 6: Assume

$$r > C\sqrt{T_M / T_m} \geq C \tag{60}$$

where T_M and T_m are the maximum and minimum eigenvalues of the following matrix:

$$T \triangleq \begin{bmatrix} P_{CRM} & 0 & 0 & 0 & 0 \\ 0 & P & 0 & 0 & 0 \\ 0 & 0 & \tilde{P} & 0 & 0 \\ 0 & 0 & 0 & \Gamma_W^{-1} & 0 \\ 0 & 0 & 0 & 0 & \Gamma_V^{-1} \end{bmatrix} \tag{61}$$

that will be used in a Lyapunov function candidate as $L = \zeta^T T \zeta$, and

$$C \triangleq \max\left[\Upsilon / \sqrt{\lambda_{min}(Q_{CRM}) - \gamma}, \Upsilon / \sqrt{\lambda_{min}(Q) - (\gamma_1 + \gamma_2)\|P\bar{B}\|}, \right.$$

$$\left. \Upsilon / \sqrt{\lambda_{min}(\tilde{Q}) - (\kappa_1 + \kappa_2)}, \Upsilon / \sqrt{k - \kappa_1 - \gamma_1 \|P\bar{B}\|}\right] \tag{62}$$

is a radius of a ball B_c containing Γ. The ball B_c is introduced to quantify β of Ω_β in Eq. (A15), where

$$\bar{Z} = \|W - W_0\|_F^2 + \|V - V_0\|_F^2, \qquad k > \kappa_1 + \gamma_1 \|P\bar{B}\|$$

$$\kappa_1 = \Theta\alpha_1 + \|P\bar{B}\|\gamma_1, \qquad \kappa_2 = \Theta\alpha_2 + \|P\bar{B}\|\gamma_2$$

$$\Theta = \|P\bar{B}\| + \|\tilde{P}\bar{B}\|, \qquad \Upsilon = \sqrt{\gamma + \gamma_2 \|P\bar{B}\| + \kappa_2 + k\bar{Z}} \tag{63}$$

The preceding quantities are used to show negativeness of the time derivative of the Lyapunov function candidate in Γ, and P, $\tilde{P} > 0$ satisfy

$$\bar{A}^T P + P\bar{A} = -Q, \qquad \tilde{A}^T \tilde{P} + \tilde{P}\tilde{A} = -\tilde{Q} \tag{64}$$

for some Q, $\tilde{Q} > 0$ with minimum eigenvalues

$$\lambda_{min}(Q) > (\gamma_1 + \gamma_2)\|P\bar{B}\|, \qquad \lambda_{min}(\tilde{Q}) > (\kappa_1 + \kappa_2) \tag{65}$$

Theorem 2: Let assumptions 1–6 hold. Consider the following weight adaptation laws:

$$\dot{V} = -\Gamma_V \left[\boldsymbol{\mu}\hat{\boldsymbol{E}}^T P\bar{B} W^T \sigma' + k(V - V_0)\right]$$

$$\dot{W} = -\Gamma_W \left[(\boldsymbol{\sigma} - \sigma' V^T \boldsymbol{\mu})\hat{\boldsymbol{E}}^T P\bar{B} + k(W - W_0)\right] \tag{66}$$

where Γ_V and $\Gamma_W > 0$, and $k > 0$. If the initial errors belong to a compact set B_r defined in Eq. (59), then the signals $\boldsymbol{E}_{CRM}$, $\boldsymbol{E}$, $\hat{\boldsymbol{E}}$, W, and V in the closed-loop system are uniformly ultimately bounded.

Proof: See the Appendix.

Remark 5: For fixed values of r and C, the inequality in condition (60) implies upper and lower bounds for the adaptation gains Γ_W and Γ_V in Eq. (66). For example, for $\Gamma_W = \gamma_W I$, and γ_W large, so that the minimum eigenvalue of T in Eq. (61) is determined by γ_W, we have $\gamma_W < r^2/(C^2 T_M)$ as an upper bound. Likewise, for small γ_W, so that the maximum eigenvalue of T is determined by the value of γ_W, we have $\gamma_W > C^2/(r^2 T_m)$ as a lower bound.

Design and Performance Results

To demonstrate that the developed approach is adaptive to both parametric uncertainty and unmodeled dynamics (including time delay), we illustrate a design and performance evaluation using a simplified model for the longitudinal dynamics of an R-50 experimental helicopter. A linear model is used both for design and simulation so as not to obscure the effects due to unmodeled dynamics and actuation limits. Figure 4 presents the implementation block diagram.

The pitch channel equations of motion of the R-50 helicopter can be expressed as a single-input/multi-output system:

$$\dot{\boldsymbol{x}} = f(\boldsymbol{x}, \delta), \qquad \begin{bmatrix} \bar{y} \\ y \end{bmatrix} = \begin{bmatrix} q \\ \theta \end{bmatrix} \tag{67}$$

where $\boldsymbol{x} = [u, q, \theta, \beta, w]^T$ is the state vector, u the forward velocity, q the pitch rate, θ the pitch angle, β the control rotor longitudinal tilt

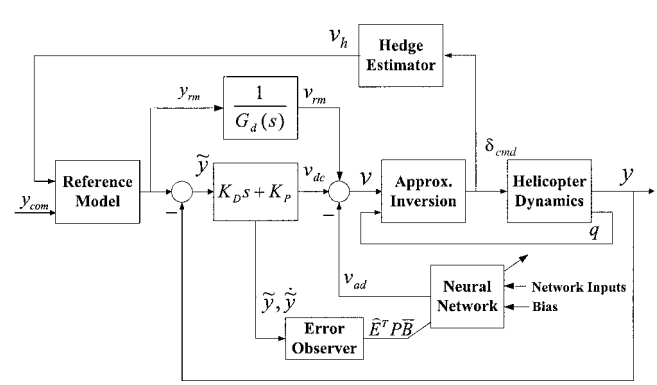

Fig. 4 Generic block diagram of single channel of adaptive attitude command system with PCH.

angle, w the vertical velocity, δ the longitudinal cyclic input (deflection angle of swashplate in radian), $\bar{y}$ an additional measurement, and y the controlled output. Note that because only pitch angle and pitch rate are used in the inversion process, the main sources of unmodeled dynamics are the control rotor dynamics and time delay.

The following linearized model was obtained based on flight-test data:

$$\begin{bmatrix} \dot{u} \\ \dot{q} \\ \dot{\theta} \\ \dot{\beta} \\ \dot{w} \end{bmatrix} = \begin{bmatrix} X_u & X_q & X_\theta & X_\beta & X_w \\ M_u & M_q & 0 & M_\beta & M_w \\ 0 & 1 & 0 & 0 & 0 \\ B_u & -1 & 0 & B_\beta & 0 \\ Z_u & Z_q & Z_\theta & Z_\beta & Z_w \end{bmatrix} \begin{bmatrix} u \\ q \\ \theta \\ \beta \\ w \end{bmatrix} + \begin{bmatrix} X_\delta \\ M_\delta \\ 0 \\ B_\delta \\ Z_\delta \end{bmatrix} \delta \quad (68)$$

where the actual coefficient values are

$$X_u = -0.0553, \quad X_q = 1.413, \quad X_\theta = -32.1731$$
$$X_\beta = -19.9033, \quad X_w = 0.0039, \quad M_u = 0.2373$$
$$M_q = -6.9424, \quad M_\beta = 68.2896, \quad M_w = 0.002$$
$$B_u = 0.0101, \quad B_\beta = -2.1633, \quad Z_u = -0.0027$$
$$Z_q = -0.0236, \quad Z_\theta = -0.2358, \quad Z_\beta = -0.1233$$
$$Z_w = -0.5727, \quad X_\delta = 11.2579, \quad M_\delta = -38.6267$$
$$B_\delta = -4.2184, \quad Z_\delta = 0.0698 \quad (69)$$

In assumption 1, we have assumed that the relative degree of the output is known. If we assume that the actuator responds to the commanded input according to the first-order dynamics

$$\tau\dot{\delta}(t) = -\delta(t) + \delta_c(t - T_D) \quad (70)$$

then θ has relative degree three.

We choose the desired linearized system in Eq. (8) so that we can stabilize the closed-loop system with the proportional–derivative controller depicted in Fig. 4:

$$G_d(s) = p/s^2(s + p) \quad (71)$$

This corresponds to $a_0 = a_1 = 0$, $a_2 = p$, and $b_0 = p$ in Eq. (8), and the error dynamics with $v_{DC} = (K_D s + K_P)e$ in Eq. (26) become

$$\left(s^3 + ps^2 + pK_D s + pK_P\right)e = 0 \quad (72)$$

The PD controller is designed to place the closed-loop poles at -20, $-8 \pm 6i$, which corresponds to $p = 36$, $K_P = 55.56$, and $K_D = 11.67$. From Eq. (10), the relationship between pseudocontrol v and the controlled output y is given by

$$p(v + \Delta) = \dddot{y} + p\ddot{y} \quad (73)$$

To get the inversion law, we are considering only q and θ, as in Eq. (74), leaving other states (u, β, w) as unmodeled dynamics:

$$\begin{bmatrix} \dot{q} \\ \dot{\theta} \end{bmatrix} = \begin{bmatrix} \hat{M}_q & 0 \\ 1 & 0 \end{bmatrix} \begin{bmatrix} q \\ \theta \end{bmatrix} + \begin{bmatrix} \hat{M}_\delta \\ 0 \end{bmatrix} \delta \quad (74)$$

We can get the approximations for $\dddot{y}$ and $\ddot{y}$ from Eq. (74):

$$\hat{\dddot{y}} = \hat{M}_q q, \qquad \hat{\ddot{y}} = \hat{M}_q^2 q + (\hat{M}_\delta/\tau)\delta_{\text{cmd}} \quad (75)$$

where $\hat{M}_q$ and $\hat{M}_\delta$ are introduced to account for parametric uncertainty in M_q and M_δ, respectively. By the use of the preceding approximation, Eq. (73) becomes

$$p(v + \Delta) = \hat{M}_q^2 q + (\hat{M}_\delta/\tau)\delta_{\text{cmd}} + p\hat{M}_q q + \Delta_3 + p\Delta_2 \quad (76)$$

where $\Delta_3 = \dddot{y} - \hat{\dddot{y}}$ and $\Delta_2 = \ddot{y} - \hat{\ddot{y}}$. By the use of Eq. (76), the approximate inversion law (5) becomes

$$\delta_{\text{cmd}} = (\tau/\hat{M}_\delta)[pv - \hat{M}_q(\hat{M}_q + p)q] \quad (77)$$

and, from Eq. (15), the model inversion error Δ can be expressed as

$$\Delta = (1/p)(\Delta_3 + p\Delta_2) = (1/p)\{\dddot{y} - \hat{\dddot{y}} + p(\ddot{y} - \hat{\ddot{y}})\} \quad (78)$$

The eigenvalues of $\tilde{A}$ in Eq. (34) have been placed to be four times faster than those of $\bar{A}$ in Eq. (32). The adaptation gains have been set to $\Gamma_V = 10I$ and $\Gamma_W = 50I$. The following sigmoidal function

$$\sigma(z) = 1/(1 + e^{-az}) \quad (79)$$

was implemented in the NN design with five hidden neurons, with activation potentials chosen to be [2, 1.6, 1.2, 0.8, 0.2]. The so-called

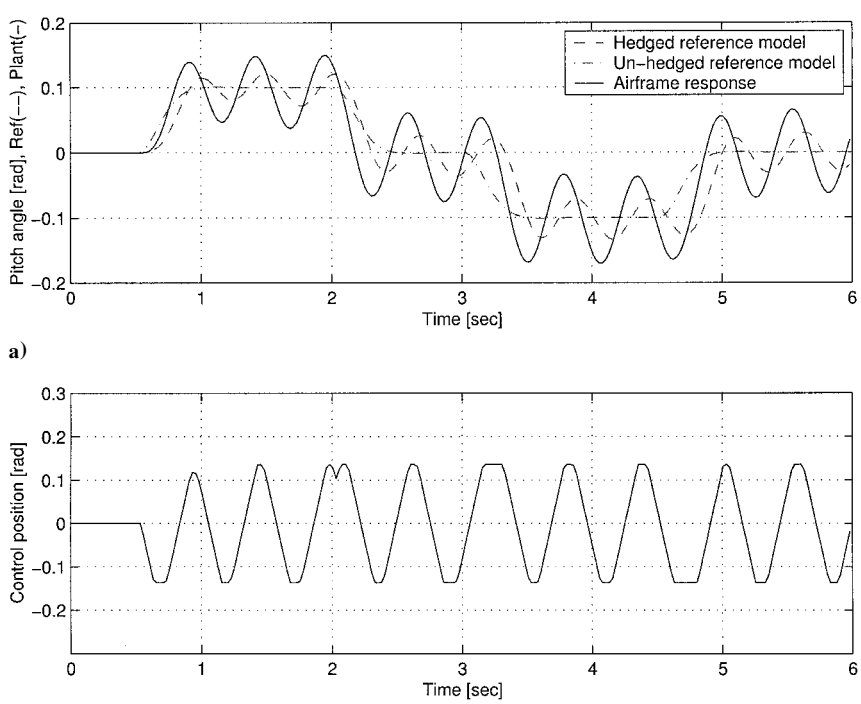

Fig. 5 Pitch tracking performance without NN controller.

σ-modification gain k in the NN update laws (66) was selected to be five. The σ-modification initial matrices W_0 and V_0 are set to zero because no a priori knowledge for estimates of the weight matrices is available. The number of neurons was chosen experimentally by starting with a large number and gradually reducing until a degradation in performance became perceptible.

As shown in Fig. 4, the commanded pitch attitude is processed through a linear third-order reference model,

$$y_{\mathrm{RM}} = [2\omega^3/(s+2\omega)(s^2+2\zeta\omega s+\omega^2)]y_{\mathrm{com}} \tag{80}$$

where $\omega = 10$ and $\zeta = 0.8$. PCH signal v_h is generated as in Eq. (49)

$$v_h = (\hat{M}_\delta/\tau p)(\delta_{\mathrm{cmd}} - \hat{\delta}) \tag{81}$$

and is multiplied by p and subtracted from the reference model output ($\ddot{y}_{\mathrm{RM}}$), which becomes the reference model state update ($\ddot{x}_{\mathrm{RM}} = \ddot{y}_{\mathrm{RM}} - pv_h$) as in Eq. (50).

Figures 5–7 provide simulated performance results of the adaptive controller using the helicopter model in Eq. (68). The simulation includes the control rotor dynamics, actuator dynamics ($\tau = 0.04$ s), time delay ($T_D = 0.03$ s), and control limits (7.8 deg in position and 78 deg/s in rate). The command to the reference model is a sequence of positive, zero, and negative steps. The parameter estimates used in Eq. (77) are $\hat{M}_\delta = 0.7M_\delta$ and $\hat{M}_q = 2M_q$.

Figure 5 presents the pitch tracking performance without NN augmentation. Figure 5a gives a comparison of the unhedged reference

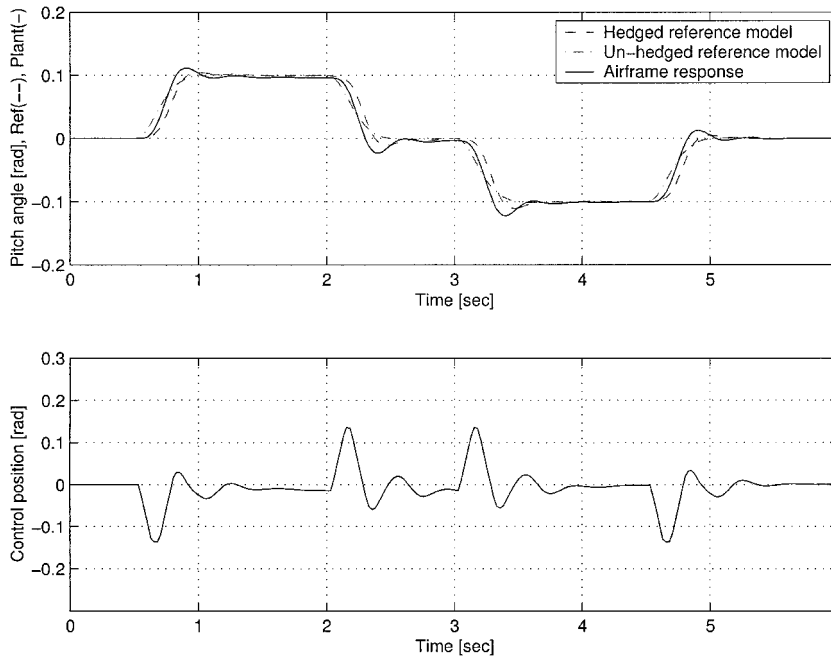

Fig. 6 Pitch tracking performance with NN controller.

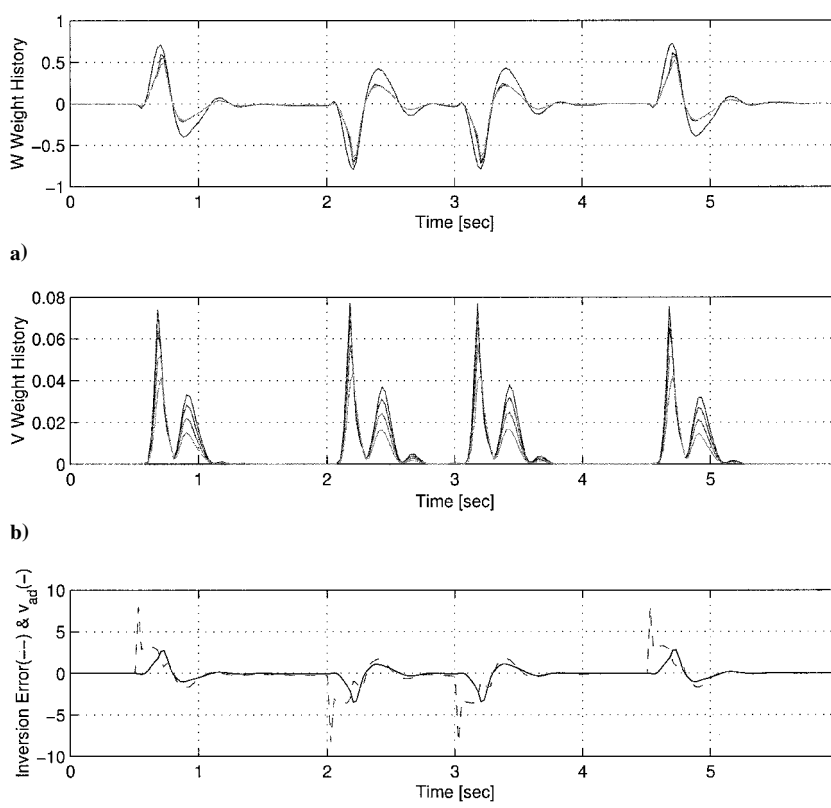

Fig. 7 NN weights (W and V) history and inversion error vs adaptive signal.

model output (dash–dot line) and the hedged reference model output (dashed line), which includes the effect of PCH, with the pitch attitude response of the airframe (solid line). The inversion error causes an unstable attitude response and commands control input (δ_{cmd}) beyond the capacity of the actuator. The PCH modifies the reference model output so that the airframe response appears to follow the hedged reference model within the capacity of the actuator. Note that the actuator response is either position or rate limited throughout the entire time interval. The airframe response without hedging is similar. The main sources of the limit-cycle behavior observed here are the unmodeled dynamics and the actuation limits.

Figure 6 repeats the plots presented in Fig. 5 with NN augmentation. Acceptable tracking of the filtered and hedged command is obtained even during brief periods where the position and rate limits are encountered. The results demonstrate the ability of the high-bandwidth flight-control system to operate at the physical limits of the aircraft hardware while delivering acceptable tracking performance. This is made possible by the introduction of hedging, which permits correct adaptation to continue while not in control. Note that the unhedged reference model outputs in Figs. 5 and 6 are identical, and the airframe response appears to lag the unhedged command for a period of time, but lead the hedged command. This behavior is a consequence of the feedforward term from the refernce model v_{RM} in Fig. 4.

Figure 7a shows the NN weights time history W (output layer) and Fig. 7b V (input layer). The weights have a tendency to return to zero after each step in command due to the σ-modification term in Eq. (66). Figure 7c shows the inversion error Δ and the output of the NN v_{ad}. Note that v_{ad} approximates Δ, except when the command is initiated, which causes slight overshoots in the pitch attitude response in Fig. 6. This demonstrates the effectiveness of PCH in allowing adaptation to continue during periods of control saturation.

Conclusions

A novel approach has been illustrated for high-bandwidth adaptive flight-control system design. A key feature is that it permits the design of stable adaptive control laws for nonlinear plants of arbitrary relative degree. The resulting controller adapts to both parametric uncertainty and unmodeled dynamics, including time delay. When combined with PCH, the approach can be used to design high-bandwidth controllers that exploit the full nonlinear capabilities of the plant and the actuators. The numerical results indicate that this is a highly effective approach to adaptive control design for UAV applications in which there is a desire to utilize the full maneuvering capability of the vehicle. Quantitatively, our results show that bandwidth can be increased, and rise time can be reduced to the minimum attainable level established by the limits of the actuation system and the inherent time delay present in the overall system.

Appendix: Proof of Theorem 2

Proof: Consider the following Lyapunov function candidate:

$$L = L_{\text{CRM}} + \boldsymbol{E}^T P \boldsymbol{E} + \tilde{\boldsymbol{E}}^T \tilde{P} \tilde{\boldsymbol{E}} + 2\,\text{tr}\left(\tilde{W}^T \Gamma_W^{-1} \tilde{W}\right) + 2\,\text{tr}\left(\tilde{V}^T \Gamma_V^{-1} \tilde{V}\right) \tag{A1}$$

where $L_{\text{CRM}} = \boldsymbol{E}_{\text{CRM}}^T P_{\text{CRM}} \boldsymbol{E}_{\text{CRM}}$ is introduced to show the boundedness of the reference model command tracking error when incorporated with PCH.

The derivative of L will be

$$\dot{L} = \dot{L}_{\text{CRM}} - \boldsymbol{E}^T Q \boldsymbol{E} - \tilde{\boldsymbol{E}}^T \tilde{Q} \tilde{\boldsymbol{E}} + 2\boldsymbol{E}^T P \bar{B}(v_{\text{ad}} - \boldsymbol{\Delta}) - 2\tilde{\boldsymbol{E}}^T \tilde{P} \bar{B}(v_{\text{ad}} - \boldsymbol{\Delta}) + 2\,\text{tr}\left(\tilde{W}^T \Gamma_W^{-1} \dot{\tilde{W}}\right) + 2\,\text{tr}\left(\tilde{V}^T \Gamma_V^{-1} \dot{\tilde{V}}\right) \tag{A2}$$

With the definition of $\tilde{\boldsymbol{E}} = \hat{\boldsymbol{E}} - \boldsymbol{E}$ and Eq. (48), this can be written

$$\dot{L} = \dot{L}_{\text{CRM}} - \boldsymbol{E}^T Q \boldsymbol{E} - \tilde{\boldsymbol{E}}^T \tilde{Q} \tilde{\boldsymbol{E}} + 2\hat{\boldsymbol{E}}^T P \bar{B}[\tilde{W}^T(\boldsymbol{\sigma} - \boldsymbol{\sigma}' V^T \boldsymbol{\mu}) + W^T \boldsymbol{\sigma}' \tilde{V}^T \boldsymbol{\mu} + \boldsymbol{w} - \boldsymbol{\epsilon}] - 2\tilde{\boldsymbol{E}}^T(\tilde{P}\bar{B} + P\bar{B})(v_{\text{ad}} - \boldsymbol{\Delta}) + 2\,\text{tr}\left(\tilde{W}^T \Gamma_W^{-1} \dot{\tilde{W}}\right) + 2\,\text{tr}\left(\tilde{V}^T \Gamma_V^{-1} \dot{\tilde{V}}\right) \tag{A3}$$

Substituting the adaptive laws implies

$$\dot{L} = \dot{L}_{\text{CRM}} - \boldsymbol{E}^T Q \boldsymbol{E} - \tilde{\boldsymbol{E}}^T \tilde{Q} \tilde{\boldsymbol{E}} + 2\hat{\boldsymbol{E}}^T P \bar{B}(\boldsymbol{w} - \boldsymbol{\epsilon}) - 2\tilde{\boldsymbol{E}}^T(\tilde{P}\bar{B} + P\bar{B})(v_{\text{ad}} - \boldsymbol{\Delta}) - 2k\,\text{tr}[\tilde{W}(W - W_0)] - 2k\,\text{tr}[\tilde{V}(V - V_0)] \tag{A4}$$

By the use of upper bounds from conditions (44) and (47), the derivative of the Lyapunov function candidate can be upper bounded as

$$\dot{L} \le \dot{L}_{\text{CRM}} - \lambda_{\min}(Q)\|\boldsymbol{E}\|^2 - \lambda_{\min}(\tilde{Q})\|\tilde{\boldsymbol{E}}\|^2 + 2\|P\bar{B}\|\|\hat{\boldsymbol{E}}\|(\gamma_1\|\tilde{Z}\|_F + \gamma_2) + 2\Theta\|\tilde{\boldsymbol{E}}\|(\alpha_1\|\tilde{Z}\|_F + \alpha_2) - \left[\|\tilde{W}\|_F^2 + \|W - W_0\|_F^2 - \left\|W^* - W_0\right\|_F^2\right] - k\left[\|\tilde{V}\|_F^2 + \|V - V_0\|_F^2 - \left\|V^* - V_0\right\|_F^2\right] \tag{A5}$$

where the following property for matrices has been used:

$$2\,\text{tr}\left[\tilde{W}^T(W - W_0)\right] = \|\tilde{W}\|_F^2 + \|W - W_0\|_F^2 - \left\|W^* - W_0\right\|_F^2 \tag{A6}$$

Furthermore,

$$\dot{L} \le \dot{L}_{\text{CRM}} - \lambda_{\min}(Q)\|\boldsymbol{E}\|^2 - \lambda_{\min}(\tilde{Q})\|\tilde{\boldsymbol{E}}\|^2 + 2\|P\bar{B}\|(\|\boldsymbol{E}\| + \|\tilde{\boldsymbol{E}}\|)(\gamma_1\|\tilde{Z}\|_F + \gamma_2) + 2\Theta\|\tilde{\boldsymbol{E}}\|(\alpha_1\|\tilde{Z}\|_F + \alpha_2) - k\|\tilde{Z}\|_F^2 + k\bar{Z} \tag{A7}$$

Grouping terms, condition (A7) can be written

$$\dot{L} \le \dot{L}_{\text{CRM}} - \lambda_{\min}(Q)\|\boldsymbol{E}\|^2 - \lambda_{\min}(\tilde{Q})\|\tilde{\boldsymbol{E}}\|^2 + 2\|P\bar{B}\|\|\boldsymbol{E}\|[\gamma_1\|\tilde{Z}\|_F + \gamma_2] + 2\|\tilde{\boldsymbol{E}}\|[\Theta(\alpha_1\|\tilde{Z}\|_F + \alpha_2) + \|P\bar{B}\|(\gamma_1\|\tilde{Z}\|_F + \gamma_2)] - k\|\tilde{Z}\|_F^2 + k\bar{Z} \tag{A8}$$

and, furthermore, put in the form

$$\dot{L} \le -\lambda_{\min}(Q_{\text{CRM}})\|\boldsymbol{E}_{\text{CRM}}\|^2 + 2\gamma\|\boldsymbol{E}_{\text{CRM}}\| - \lambda_{\min}(Q)\|\boldsymbol{E}\|^2 - \lambda_{\min}(\tilde{Q})\|\tilde{\boldsymbol{E}}\|^2 + 2\|P\bar{B}\|\|\boldsymbol{E}\|[\gamma_1\|\tilde{Z}\|_F + \gamma_2] + 2\|\tilde{\boldsymbol{E}}\|[\kappa_1\|\tilde{Z}\|_F + \kappa_2] - k\|\tilde{Z}\|_F^2 + k\bar{Z} \tag{A9}$$

Utilize the following inequalities:

$$\begin{aligned} 2\gamma\|\boldsymbol{E}_{\text{CRM}}\| &\le \gamma\left(\|\boldsymbol{E}_{\text{CRM}}\|^2 + 1\right) \\ 2\gamma_1\|P\bar{B}\|\|\boldsymbol{E}\|\|\tilde{Z}\|_F &\le \gamma_1\|P\bar{B}\|(\|\boldsymbol{E}\|^2 + \|\tilde{Z}\|^2) \\ 2\gamma_2\|P\bar{B}\|\|\boldsymbol{E}\| &\le \gamma_2\|P\bar{B}\|(\|\boldsymbol{E}\|^2 + 1) \\ 2\kappa_1\|\tilde{E}\|\|\tilde{Z}\|_F &\le \kappa_1(\|\tilde{\boldsymbol{E}}\|^2 + \|\tilde{Z}\|^2) \\ 2\kappa_2\|\tilde{\boldsymbol{E}}\| &\le \kappa_2(\|\tilde{\boldsymbol{E}}\|^2 + 1) \end{aligned} \tag{A10}$$

On completion of squares, we get the following upper bound:

$$\dot{L} \le -[\lambda_{\min}(Q_{\text{CRM}}) - \gamma]\|\boldsymbol{E}_{\text{CRM}}\|^2 - [\lambda_{\min}(Q) - (\gamma_1 + \gamma_2)\|P\bar{B}\|]\|\boldsymbol{E}\|^2 - [\lambda_{\min}(\tilde{Q}) - (\kappa_1 + \kappa_2)]\|\tilde{\boldsymbol{E}}\|^2 - (k - \kappa_1 - \gamma_1\|P\bar{B}\|)\|\tilde{Z}\|_F^2 + k\bar{Z} + \gamma + \gamma_2\|P\bar{B}\| + \kappa_2 \tag{A11}$$

One of the following conditions

$$\begin{aligned} \|\boldsymbol{E}_{\text{CRM}}\| &> \Upsilon \Big/ \sqrt{\lambda_{\min}(Q_{\text{CRM}}) - \gamma} \\ \|\boldsymbol{E}\| &> \Upsilon \Big/ \sqrt{\lambda_{\min}(Q) - (\gamma_1 + \gamma_2)\|P\bar{B}\|} \\ \|\tilde{\boldsymbol{E}}\| &> \Upsilon \Big/ \sqrt{\lambda_{\min}(\tilde{Q}) - (\kappa_1 + \kappa_2)} \\ \|\tilde{Z}\|_F &> \Upsilon \Big/ \sqrt{k - \kappa_1 - \gamma_1\|P\bar{B}\|} \end{aligned} \tag{A12}$$

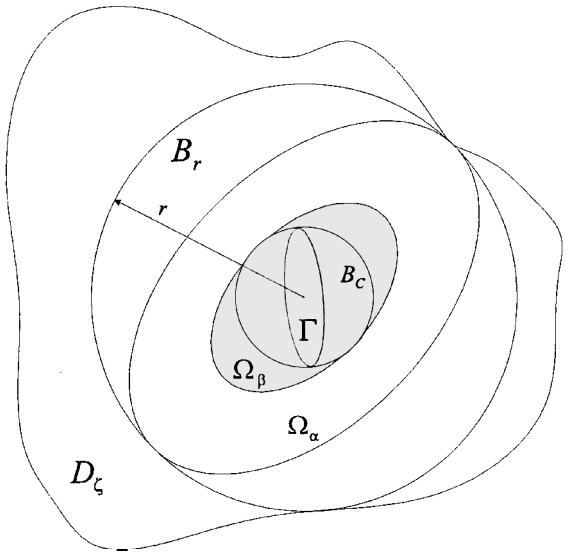

Fig. A1 Geometric representation of the sets in the error space.

will render $\dot{L} < 0$ outside a compact set, where $\Upsilon = \sqrt{(\gamma + \gamma_2 \|P\bar{B}\| + \kappa_2 + k\bar{Z})}$.

To ensure that the conditions (A12) define a compact set in the space of error variables, write condition (A11) in the following way, such that the condition $\dot{L} < 0$ is true everywhere in the space of error variables $\boldsymbol{E}_{\mathrm{CRM}}$, $\boldsymbol{E}$, $\tilde{\boldsymbol{E}}$, and $\tilde{Z}$, outside the ellipsoid Γ:

$$[\lambda_{\min}(Q_{\mathrm{CRM}}) - \gamma]\|\boldsymbol{E}_{\mathrm{CRM}}\|^2 + [\lambda_{\min}(Q) - (\gamma_1 + \gamma_2)\|P\bar{B}\|]\|\boldsymbol{E}\|^2 + [\lambda_{\min}(\tilde{Q}) - (\kappa_1 + \kappa_2)]\|\tilde{\boldsymbol{E}}\|^2 + (k - \kappa_1 - \gamma_1\|P\bar{B}\|)\|\tilde{Z}\|_F^2 = \Upsilon^2 \tag{A13}$$

Define a compact set in the space of the error variables ζ,

$$B_C = \{\zeta \in B_r : \|\zeta\| \leq C\} \tag{A14}$$

containing Γ, outside of which $\dot{L} < 0$. Note from Eq. (60) that $B_C \subset B_r$. Consider the Lyapunov function candidate in Eq. (A1) and write it as

$$L = \zeta^T T \zeta$$

Let β be the maximum value of the Lyapunov function L on the edge of B_C:

$$\beta \triangleq \max_{\|\zeta\| = C} L = C^2 T_M \tag{A15}$$

Introduce the set, depicted in Fig. A1:

$$\Omega_\beta = \{\zeta : L \leq \beta\} \tag{A16}$$

Let α be the minimum value of the Lyapunov function L on the edge of B_r:

$$\alpha \triangleq \min_{\|\zeta\| = r} L = r^2 T_m \tag{A17}$$

Define the compact set

$$\Omega_\alpha = \{\zeta \in B_r : L \leq \alpha\} \tag{A18}$$

The condition in condition (60) ensures that $B_C \subset \Omega_\beta \subset \Omega_\alpha$ and, thus, the ultimate boundedness of ζ.

Acknowledgments

This work is supported in part by the U.S. Army Research Office under Contract NCC 2-945 and the U.S. Air Force Office of Scientific Research under Contract F49620-98-1-0437. The authors would like to acknowledge the contributions of Eric Johnson of Georgia Institute of Technology and Flavio Nardi of Fiat Auto Research and Development.

References

[1]Isidori, A., *Nonlinear Control Systems*, Springer, Berlin, 1995, Chap. 4.2.

[2]Khalil, H., *Nonlinear Systems*, Prentice–Hall, Upper Saddle River, NJ, 1996, Chap. 12.

[3]Kim, B., and Calise, A., "Nonlinear Flight Control Using Neural Networks," *Journal of Guidance, Control, and Dynamics*, Vol. 20, No. 1, 1997, pp. 26–33.

[4]Chen, F. C., and Khalil, H. K., "Adaptive Control of Nonlinear Systems Using Neural Networks," *International Journal of Control*, Vol. 55, No. 6, 1992, pp. 1299–1317.

[5]Yesildirek, A., and Lewis, F., "Feedback Linearization Using Neural Networks," *Automatica*, Vol. 31, No. 11, 1995, pp. 1659–1664.

[6]Lewis, F., Jagannathan, S., and Yesildirek, A., *Neural Network Control of Robot Manipulators and Nonlinear Systems*, Taylor and Francis, Philadelphia, 1999, Chap. 5.

[7]Leitner, J., Calise, A., and Prasad, J., "Analysis of Adaptive Neural Networks for Helicopter Flight Control," *Journal of Guidance, Control, and Dynamics*, Vol. 20, No. 5, 1997, pp. 972–979.

[8]Rysdyk, R., and Calise, A. J., "Adaptive Model Inversion Flight Control for Tiltrotor Aircraft," *Journal of Guidance, Control, and Dynamics*, Vol. 22, No. 3, 1999, pp. 402–407.

[9]McFarland, M., and Calise, A., "Multilayer Neural Networks and Adaptive Control of Agile Anti-Air Missile," *Journal of Guidance, Control, and Dynamics*, Vol. 23, No. 3, 2000, pp. 547–553.

[10]Calise, A., Lee, S., and Sharma, M., "Development of a Reconfigurable Flight Control Law for a Tailless Aircraft," *Journal of Guidance, Control, and Dynamics*, Vol. 24, No. 5, 2001, pp. 896–902.

[11]Kim, Y., and Lewis, F., *High Level Feedback Control with Neural Networks*, World Scientific, Singapore, Republic of Singapore, 1998, Chap. 3.

[12]Hovakimyan, N., Rysdyk, R., and Calise, A., "Dynamic Neural Networks for Output Feedback Control," *Proceedings of the Conference on Decision and Control*, Vol. 2, Inst. of Electrical and Electronics Engineers, Piscataway, NJ, 1999, pp. 1685–1690.

[13]Hovakimyan, N., Nardi, F., Calise, A., and Lee, H., "Adaptive Output Feedback Control of a Class of Nonlinear Systems," *International Journal of Control*, Vol. 74, No. 12, 2001, pp. 1161–1169.

[14]Hovakimyan, N., Nardi, F., Calise, A., and Kim, N., "Adaptive Output Feedback Control of Uncertain Systems Using Single Hidden Layer Neural Networks," *IEEE Transactions on Neural Networks* (to be published).

[15]Johnson, E., and Calise, A., "Neural Network Adaptive Control of Systems with Input Saturation," *Proceedings of the American Control Conference*, Inst. of Electrical and Electronics Engineers, Piscataway, NJ, 2001, pp. 3527–3532.

[16]Corban, J. E., Calise, A., Prasad, J., Hur, J., and Kim, N., "Flight Evaluation of Adaptive High-Bandwidth Control Methods for Unmanned Helicopters," *Proceedings of the AIAA Guidance, Navigation, and Control Conference*, AIAA, Reston, VA, 2002.

[17]Hovakimyan, N., and Calise, A., "Adaptive Output Feedback Control of Uncertain Multi-Input Multi-Output Systems Using Single Hidden Layer Neural Networks," *International Journal of Control* (submitted for publication).

[18]Calise, A., Hovakimyan, N., and Idan, M., "Adaptive Output Feedback Control of Nonlinear Systems Using Neural Networks," *Automatica*, Vol. 37, No. 8, 2001, pp. 1201–1211.

[19]Lewis, F., Yesildirek, A., and Liu, K., "Multilayer Neural-Net Robot Controller with Guaranteed Tracking Performance," *IEEE Transactions on Neural Networks*, Vol. 7, No. 2, 1996, pp. 388–399.

[20]Hovakimyan, N., Nardi, F., and Calise, A., "A Novel Observer Based Adaptive Output Feedback Approach for Control of Uncertain Systems," *Proceedings of the American Control Conference*, Inst. of Electrical and Electronics Engineers, Piscataway, NJ, 2001, pp. 2444–2449.

[21]Cybenko, G., "Approximation by Superpositions of Sigmoidal Function," *Mathematics of Control, Signals and Systems*, Vol. 2, No. 4, 1989, pp. 303–314.